IOPscience iopscience.iop.org

Home Search Collections Journals About Contact us My IOPscience

Thermal nanoimprint process for high-temperature fabrication of mesoscale epitaxial exchange-biased metallic wire arrays

This article has been downloaded from IOPscience. Please scroll down to see the full text article.

2011 J. Micromech. Microeng. 21 045024

(http://iopscience.iop.org/0960-1317/21/4/045024)

View the table of contents for this issue, or go to the journal homepage for more

Download details:
IP Address: 173.250.148.179
The article was downloaded on 02/06/2011 at 17:58

Please note that terms and conditions apply.

IOP PUBLISHING JOURNAL OF MICROMECHANICS AND MICROENGINEERING

J. Micromech. Microeng. **21** (2011) 045024 (7pp) doi:10.1088/0960-1317/21/4/045024

Thermal nanoimprint process for high-temperature fabrication of mesoscale epitaxial exchange-biased metallic wire arrays

W Zhang[1], D N Weiss[2,3] and K M Krishnan[1]

[1] Department of Materials Science and Engineering, University of Washington, Seattle, WA 98195, USA
[2] Washington Technology Center, Seattle, WA 98195, USA
[3] Department of Electrical Engineering, University of Washington, Seattle, WA 98195, USA

E-mail: kannanmk@uw.edu

Received 19 November 2010, in final form 21 January 2011
Published 17 March 2011
Online at stacks.iop.org/JMM/21/045024

Abstract

A thermal nanoimprint process for the high-temperature (400 °C) fabrication of submicron, epitaxial, metallic wire arrays over areas $> 1 \times 1$ cm^2 is reported. Based on a method using an imprinted polymeric bilayer resist template that is transferred to a metallic (molybdenum) mask, this process is enabled by an appropriate undercut profile of the Mo mask. The undercut profile is obtained from a distinctive wedge-shaped profile of the polymeric resist layers by carefully controlling the etch parameters. Using flexible ethylene tetrafluoroethylene imprint molds, we demonstrate defect-free imprinting on MgO substrates. Epitaxial patterning is demonstrated with Fe/MnPd bilayer wire arrays subsequently grown along well-defined crystallographic orientations. X-ray diffraction of the patterned arrays reveals that the MnPd can be grown in two different crystallographic orientations (*c*-axis and *a*-axis normals). The epitaxial nature of the patterned arrays is further confirmed by magnetic measurements that demonstrate the competing effects of intrinsic (magnetocrystalline and exchange) and lithography-induced shape anisotropies on the magnetization reversal characteristics along different directions with respect to the axis of the wire arrays.

(Some figures in this article are in colour only in the electronic version)

1. Introduction

The control of the magnetic anisotropy and domain configuration in patterned magnetic elements is of great importance for spintronics devices. In particular, lithographically defined planar wires in the mesoscopic scale have been widely investigated because of their potential applications in data storage [1] and logic [2] devices. The mesoscale (100–1000 nm), which is the size range where different magnetic anisotropies can compete, is of particular research interest, with most of the reported work focused on patterned wires from polycrystalline films. In contrast, patterned wires from epitaxial single-crystalline magnetic thin films, also in the mesoscopic scale, have been fabricated in a few cases [3–5], to study more technologically important magnetic properties, not easily accessible in their polycrystalline counterparts, such as magnetocrystalline anisotropy [3], magneto-elastic coupling [4], and ferromagnetic/antiferromagnetic interface spin structures [5]. Additional functionality in magnetic memory devices and spintronics devices can be achieved by epitaxial growth (tuning the magnetocrystalline anisotropy) and patterning wire arrays (lithographically-induced shape anisotropy). Therefore, reliable and economical methods to fabricate large area, high quality epitaxial submicron wires are greatly desired for model studies and technological developments.

 © 2011 IOP Publishing Ltd Printed in the UK & the USA

Direct fabrication of such patterned elements over sufficiently large areas is not straightforward. Typical methods involve indirect patterning, such as ion-milling of pre-deposited films through etch masks generated by conventional lithography [3–5]. Conventional lithography techniques are not suitable for direct-patterning epitaxial films because polymeric resists are not compatible with the high temperatures required for substrate cleaning and subsequent epitaxial film growth. Nanoimprint lithography (NIL) [6] has recently been demonstrated as an efficient tool for large-area patterning of non-epitaxial magnetic structures, with specific advantages over both photolithography and e-beam lithography [7, 8]. Suzuki *et al* (2008) recently introduced a NIL process compatible with epitaxial film materials, in which the polymeric resist mask was transferred to a high-temperature-stable molybdenum (Mo) mask prior to metal epitaxy [9]. However, they have demonstrated this process only for very thin films of one single material, and the liftoff quality seemed to be imperfect with rough edges as revealed by scanning electron microscopy (SEM) images. Structural defects, such as those generated during nanofabrication, can have significant influence on magnetic properties [10] including their magnetic reversal characteristics. As far as possible, defect-free epitaxial elements are desirable to provide reliable magnetic behavior. Here, we report a significantly improved method that, by carefully controlling the parameters for dry etching and developing, creates a distinctive wedge-shaped profile in the polymeric sacrificial resist layer; this profile is then transferred to the all-metallic Mo resist, which shows an undercut profile. This Mo undercut profile significantly improves the quality of the liftoff process for the final epitaxial magnetic structures. Using this technique, we demonstrate NIL-based patterning of epitaxial heterostructured Fe/MnPd bilayer thin-film wire arrays on MgO with controlled crystallographic orientation. Fe/MnPd is an epitaxial exchange bias system [11–14] with many interesting magnetic properties including asymmetric magnetization reversal [15], stepped hysteresis loops [16], interfacial rotatable antiferromagnetic spins [17] and low temperature spin re-orientation [18]. In the Fe/MnPd wire arrays, the magnetization reversal processes are controlled by the intrinsic magnetocrystalline anisotropy of Fe (K_1), the uniaxial shape anisotropy (K_u) of the wires, as well as the exchange anisotropy (K_{eb}) originated from the Fe/MnPd interface.

The ability to achieve such high-quality epitaxial metallic structures offers a unique opportunity to study the interplay between competing magnetic anisotropies (both intrinsic and lithographically induced). Here, we also present the magnetization reversal behavior of our Fe/MnPd submicron wire arrays with competing magnetic anisotropies, measured by a vibrating sample magnetometer (VSM) and anisotropic magnetoresistance (AMR). The AMR of magnetic wire arrays has been rarely studied [19] and no report has been focused on epitaxial samples. In our measurement, different magnetization reversal characteristics, i.e. domain wall (DW) nucleation and coherent rotation, are observed at parallel and perpendicular directions to the wires, respectively, driven by different combinations of anisotropy easy axes.

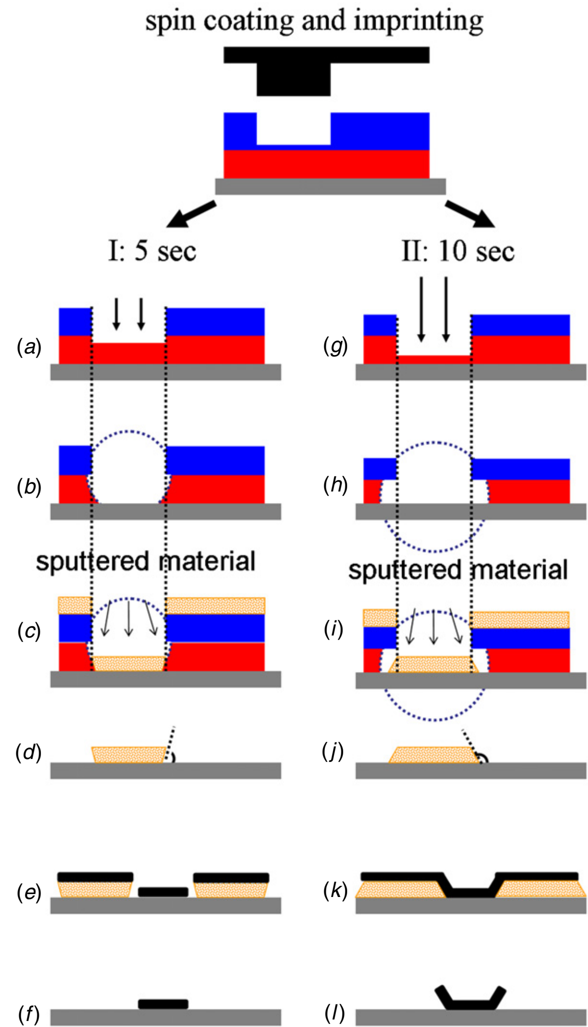

Figure 1. Illustration of our refined NIL process P_I for epitaxial magnetic patterning with a short 5 s dry-etch step (*a*)–(*f*) and a conventional process P_{II} with a longer 10 s dry-etch step. The circles in (*b*) and (*h*) show the edge of isotropic removal of the polymeric sacrificial resist layer during developing. Blue: thermal imprint resist; red: polymeric undercut resist; orange: Mo hard mask; black: magnetic multilayer film; gray: substrate.

2. Process description

Figure 1(*a*)–(*f*) shows a schematic of our process for obtaining a Mo mask with the right undercut profile and the subsequent clean liftoff for epitaxial film structures. A bilayer of polymeric undercut resist and thermal imprint resist is thermally imprinted with an appropriate mold. A brief anisotropic de-scum etch step removes the residue of the imprint resist and a certain amount of the undercut resist, figure 1(*a*). The undercut resist is then wet etched appropriately to develop a wedge-shaped resist profile. Since the wet-etch proceeds in a nearly isotropic manner, the etched resist profile therefore can be approximated by a circle, with the center located at the start point of the etch, figure 1(*b*). The following attributes are crucial for the success of our process, which is totally controllable by this two-step etch procedure: the start point of the wet-etch must be close to the top surface of the undercut resist layer and the radius of the

circle defining the etching front, determined by the etch time, must be almost equal to the distance between the etch start point and the substrate. These are the key factors to obtain the wedge-shaped profiles. The Mo layer is then deposited, figure 1(*c*), followed by the polymer-resist liftoff. The wedge-shaped resist produces an undercut profile of the Mo mask, figure 1(*d*). Epitaxial material is then deposited at high temperature onto the Mo template, figure 1(*e*), followed by the Mo liftoff in the H_2O_2 solution, to complete the process. Due to the Mo undercut, very clean liftoff can be obtained and high quality epitaxial patterned structures can be produced.

The duration of the de-scum etch step in figure 1(*a*) is the key to obtain the desired wedge-shaped polymer resist profile. We demonstrate this in figures 1(*g*)–(*l*) for a de-scum etch duration increased by a factor 2. This process creates a conventional undercut in the polymer bilayers; however, it does not create the desired undercut in the Mo mask. The process described by Suzuki *et al* [9], which uses an even longer anisotropic de-scum etch to remove the entire undercut resist layer underneath the imprinted area, is similar to this process. In brief, the start point of the wet-etch is moved downward, deep into the undercut resist layer by the longer anisotropic de-scum etch. After the wet-etch, as revealed by the circle, a conventional bilayer resist undercut is created, figure 1(*h*). Similarly, the Mo layer is subsequently deposited, figure 1(*i*), followed by the resist liftoff to complete the mask transfer, figure 1(*j*). Epitaxial material is deposited at high temperature onto the Mo template, figure 1(*k*). Finally, the Mo layer is removed in the H_2O_2 solution. Since the Mo mask does not have an undercut profile, the liftoff process often needs to be assisted with ultrasonication [9]. As a consequence, only very thin epitaxial films can be deposited without the creation of rough edges in the patterned structures, otherwise, the liftoff result would be affected, figure 1(*l*).

3. Experiment

3.1. Fabrication process on a Si substrate

The process was first developed on a Si substrate. Polymeric undercut resist LOR 1A (MicroChem Corp., Newton, MA) and thermal imprint resist NXR-1025 (Nanonex, Monmouth Junction, NJ) were spin-coated on a Si wafer. Each layer was soft-baked on a hotplate subsequent to coating. The undercut resist was baked at 200 °C for 10 min and the imprint resist was baked at 150 °C for 90 s. The thicknesses of the resist layers are 100 and 60 nm for LOR 1A and NXR-1025, respectively. Next, the coated wafer was thermally imprinted using a Si mold (12.5 × 12.5 mm^2 patterned areas, 200 nm groove depth, 833 nm period square gratings with 50% duty cycle from LightSmyth Technologies, Inc., Eugene, OR) in a Nanonex NX-B100 compact thermal nanoimprinter. The sample was maintained at 120 °C and 200 psi during a 60 s imprint process. The imprint layer almost doubled its thickness after imprinting and only very thin residues were left on the imprinted trenches, which is due to the relatively large groove depth (200 nm) of the mold compared with the NXR-1025 layer thickness (60 nm). The imprinted wafer was then broken into two pieces (P_I and P_{II}) for different subsequent treatments. Anisotropic oxygen-plasma reactive ion etching (RIE) was performed on P_I and P_{II} at 25 W for 5 s and 10 s, respectively (Trion Phantom II). Next, an isotropic wet-etch using tetramethylammonium hydroxide (TMAH, from MicroChem Corp.), with high etch selectivity for LOR 1A, was carried out for each sample to further remove the undercut layer and expose the Si substrates. The patterned resist templates were then taken into an ion-beam sputtering (IBS) chamber to deposit a Mo mask ∼70 nm thick. After resist liftoff in Remover PG (MicroChem Corp.), Mo masks were obtained on the substrate thereby completing the mask transfer. Magnetic epitaxial Fe (10 nm)/MnPd (10 nm) bilayers were deposited onto the Mo mask at an elevated temperature (400 °C). The Mo mask was removed ultrasonically in the 30% H_2O_2 solution in the final liftoff step.

3.2. Fabrication process on MgO substrates

A similar process was conducted on single crystal MgO substrates. Clean 1″ × 1″ square MgO(0 0 1) substrates (MTI Corp., Richmond, CA) were first placed on a hotplate at 200 °C for 10 min to remove the absorbed water. Bilayer resist coating and imprinting were performed as described in section 3.1. It should be noted that the mold was placed with the wire direction parallel to the diagonal of the MgO substrates during imprinting, which resulted in the wire direction being collinear with the easy axis of Fe. After imprinting, we found that the demolding of Si molds from MgO substrates was more difficult than from Si substrates, which also increased the defect generation during the process. Demolding was easier with a flexible mold material, ethylene tetrafluoroethylene (ETFE), through a peeling process [20]. However, the transparency of both MgO and ETFE may lead to inefficient absorption of the infrared (IR) light. To overcome this, a 3″ clean Si wafer is placed on the back of the MgO substrate while mounting it together with ETFE molds to improve the IR light absorption. The temperature is stable during the whole imprint process. Defect-free imprints as large as the mold size can be fabricated. We fabricated the ETFE imprint molds by hot embossing ETFE sheets using the Si stamps as the master molds. The detailed process for replicating ETFE molds with Si stamps is described elsewhere [21]. Subsequent to imprinting, 5 s RIE dry-etching was performed, followed by wet developing to create the desired wedge-shaped resist profile. Next, a Mo layer of ∼70 nm was deposited via IBS, followed by resist liftoff in Remover PG. Magnetic bilayers, Fe (10 nm)/MnPd (10 nm), were deposited with *c*-axis and *a*-axis normal orientations, according to well-defined recipes [12, 13], on different substrates, respectively. Before the deposition of Fe/MnPd, the substrates were first heated up to 580 °C for 1.5 h *in situ* cleaning. The *c*-axis samples were deposited at 400 °C and no further annealing treatment need to be conducted. The *a*-axis samples were deposited at 120 °C and post-annealed at 250 °C for 1 h. The growth parameters are also summarized in table 1. The Mo masks were then removed in the 30% H_2O_2 solution. The

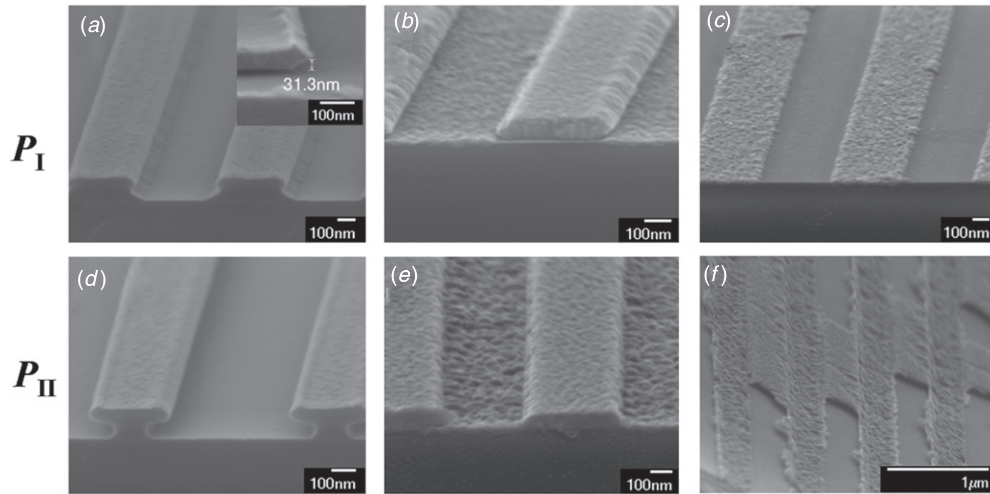

Figure 2. Scanning electron microscopy (SEM) images showing our NIL process on sample P_I with (*a*) wedge-shaped polymer bilayer, inset: Mo mask with undercut; (*b*) magnetic materials deposited onto the Mo mask with undercut, and (*c*) successful liftoff; and the conventional NIL process on sample P_{II} with (*d*) polymer undercut profile; (*e*) magnetic materials deposited onto the Mo mask without undercut, and (*f*) poor liftoff.

Table 1. Growth parameters and XRD characterizing peaks of *c*-axis and *a*-axis Fe/MnPd bilayers.

Sample	Epitaxial relationship	Deposition temperature (°C)	Post-annealing temperature (°C)	XRD peaks
c-axis	MgO(0 0 1)/Fe(0 0 1)/MnPd(0 0 1)	400	N/A	MnPd(0 0 1), MnPd(0 0 2), Fe(0 0 2)
a-axis	MgO(0 0 1)/Fe(0 0 1)/MnPd(1 0 0)	90–120	250	MnPd(2 0 0), Fe(0 0 2)

epitaxial Fe/MnPd metallic wire arrays were characterized by x-ray diffraction (XRD, Rigaku RU-200BH) using Cu Kα radiation (λ = 1.54 Å). Magnetic measurements were performed by VSM and AMR at 10 K with an in-plane rotator, both using a Quantum Design physical property measurement system (PPMS).

4. Results and discussion

4.1. Fabrication

SEM images were taken after the wet-etch of the polymer resists for samples P_I and P_{II}. Following the process described in section 3.1, different resist profiles for P_I and P_{II} were experimentally obtained. Specifically, P_I exhibited the wedge-shaped polymer-resist profile, figure 2(*a*); P_{II}, on the other hand, showed a conventional undercut, figure 2(*d*). The different resist profiles significantly affected the cross-sectional profiles of the Mo structures that were subsequently deposited. The desired undercut profile was obtained for sample P_I, figure 2(*a*), inset, which is critical for the following epitaxial patterning process. SEM images were also taken after the deposition of the magnetic materials on the Mo masks. For sample P_I, due to the undercut profile, the magnetic material deposited on top of the Mo mask does not connect with those at the bottom, which is desirable for subsequent liftoff (figure 2(*b*)). For sample P_{II} without the Mo undercut profile, the magnetic materials formed a continuous layer on the Mo masks, as shown in figure 2(*e*).

The important role of the Mo undercut profile was demonstrated by the different final liftoff results of P_I and P_{II}. For P_I, the liftoff process was completed in just a few seconds and no ultrasonication was applied. This prompt liftoff process efficiently reduced the possibility of damage to the magnetic layers. High quality Fe/MnPd metallic wires were obtained for sample P_I, as shown in figure 2(*c*). For P_{II}, the Mo mask, with the surplus magnetic materials on top, could not be removed in the H_2O_2 solution unless ultrasonication was applied for ∼2 min. After liftoff, Mo residues can still be observed in between and along the metallic wires, figure 2(*f*). The magnetic layers are also likely damaged to a certain degree by the strongly oxidizing H_2O_2 during the long ultrasonication, as revealed by the rough edges of the wires in the SEM image.

As described in section 3.2, the wedge-shaped resist was also created on MgO substrates, figure 3(*a*). The resulting Mo mask undercut profile leads to easy Mo liftoff in H_2O_2 by just shaking the substrate in the solution for a few seconds. Defect-free Fe/MnPd epitaxial metallic wire arrays were obtained on the MgO substrate, figure 3(*b*). The photograph in figure 3(*c*) shows the large area on MgO (figure 3(*c*), after Mo deposition) due to the application of ETFE soft molds.

As we have demonstrated with both Si and MgO substrates, this NIL process works well for submicron wires which are of particular interest in studies of magnetism and related spintronics devices. Nevertheless, our process, especially with the MgO substrate and ETFE mold replica, is broad and general, and in addition to magnetism, can

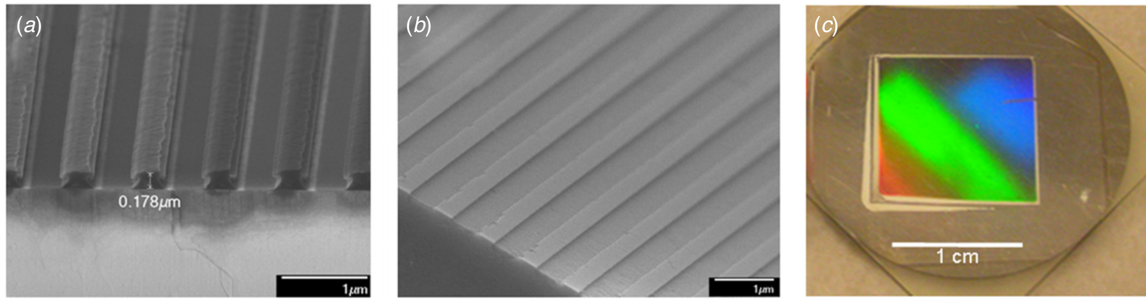

Figure 3. (*a*) Wedge-shaped polymer bilayer resist on the MgO substrate; (*b*) high resolution epitaxial Fe/MnPd wire arrays on MgO and (*c*) photographic picture of large area imprinted polymer wire arrays (after Mo deposition).

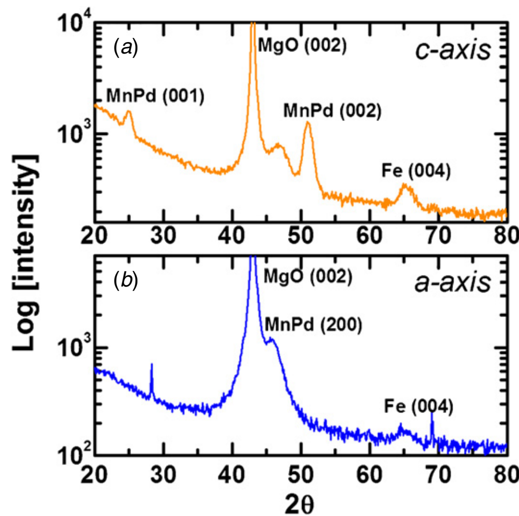

Figure 4. X-ray θ–2θ diffraction scans of *c*-axis and *a*-axis Fe/MnPd bilayer metallic wire arrays.

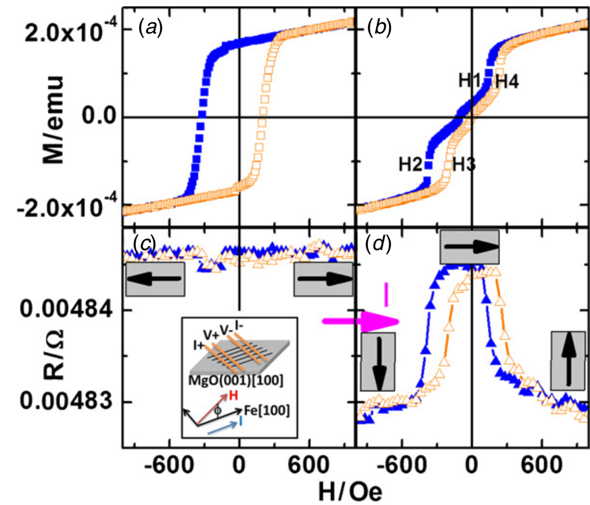

Figure 5. $M(H)$ curves measured at 10 K with (*a*) parallel and (*b*) perpendicular field cooling. $R(H)$ curves measured at 10 K with (*c*) parallel and (*d*) perpendicular field cooling. The magnetization orientation is represented by the black arrow enclosed in a square. The inset is a schematic illustration of the AMR measurement setup.

be widely applied to other epitaxial patterning purposes in superconductors and multiferroics where MgO and other similar substrates, such as Al_2O_3 and $BaTiO_3$ [9], are used. However, as our process relies on accurate control of the undercut profile of the resist bilayer, currently it precludes making structures with much smaller lateral dimensions [22], or high-aspect-ratio features, due to the mechanical instability of the resist features with the undercut.

4.2. Crystallographic characterization

The NIL-based epitaxial patterning is demonstrated with epitaxial Fe/MnPd bilayer wire arrays. Previous results [12] have shown that the antiferromagnetic MnPd can be grown with two different orientations, the *c*-axis and *a*-axis normal to the film plane, with the epitaxial relationship MgO(0 0 1)[1 0 0] ∥ Fe(0 0 1)[1 1 0] ∥ MnPd(0 0 1) and MgO(0 0 1)[100] ∥ Fe(0 0 1)[110] ∥ MnPd(1 0 0), respectively. The growth of the two orientations requires different deposition temperatures and post-annealing treatments, as described in section 3.2. The XRD θ–2θ scans of *c*-axis and *a*-axis oriented Fe/MnPd metallic wire arrays are shown in figure 4. The different normal orientations were confirmed by the corresponding characterizing peaks.

4.3. Magnetic measurements

As mentioned earlier, structural and magnetic properties are closely related in magnetic patterned elements, especially for epitaxial samples [3, 10]. We illustrate this by briefly discussing the magnetic properties of our epitaxial wire arrays, which also provides additional insight into the NIL process. For example, we present the magnetic properties of *a*-axis Fe/MnPd wire arrays, probed by VSM, $M(H)$, and AMR, $R(H)$. The sample was first field-cooled under a magnetic field, $H_{cool} = 2$ T, from 300 to 10 K, below the blocking temperature $T_B \sim 90$ K of the *a*-axis Fe/MnPd [18]. The field cooling process is performed in two different modes with H_{cool} either parallel or perpendicular to the wire direction, respectively. Both the magnetization and resistance, versus the field, i.e. $M(H)$ and $R(H)$, were measured at 10 K subsequent to each field-cooling process.

For parallel cooling and measurement, a broad hysteresis loop with one-step magnetic reversal was observed by VSM (figure 5(*a*)), showing that the magnetization reversal occurred by DW nucleation [3]. An exchange bias field, H_{eb}, ~56 Oe was observed, which can be related to K_{eb} through

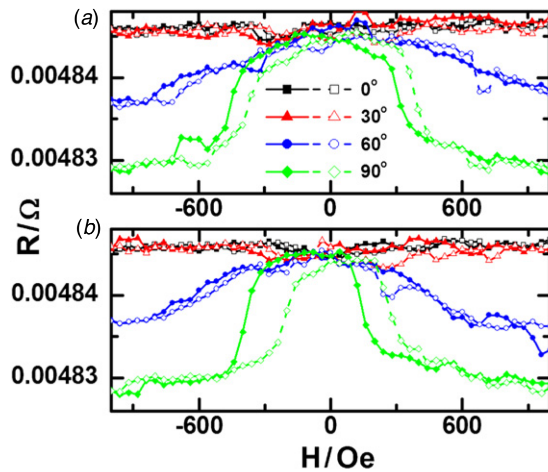

Figure 6. $R(H)$ curves measured at 10 K for the decreasing field (solid) and the increasing field (open) with parallel field cooling (*a*), and perpendicular field cooling (*b*), at selective angles, $\phi = 0°$, 30°, 60° and 90°, with respect to the wire axis.

$K_{eb} = H_{eb}M_s$, where M_s is the saturation magnetization per unit volume. The coercivity is ~265 Oe, more than one order of magnitude higher than that of the continuous films [23]. For perpendicular cooling and measurement, the efficiency of the applied field to unpin a wall trapped in a pinning center decreases and the magnetization reversal via coherent rotation becomes more effective [3, 24]. This is evidenced by the gradual reversal behavior of the $M(H)$ curve (figure 5(*b*)). However, different from the polycrystalline nanowires [24], small magnetization jumps were observed in our epitaxial ones, which took place at H_1 ~137 Oe, H_2 ~−371 Oe for descending branch, and $H_3 \sim -210$ Oe, $H_4 \sim 233$ Oe for ascending branch, respectively. These jumps indicate the rapid relaxation of the magnetization along the wire direction, due to the collinear easy axes of the Fe magnetocrystalline anisotropy and the shape anisotropy. In other words, due to the superimposed easy axes of K_1 and K_u, the magnetization relaxes more abruptly along our epitaxial wires than in the polycrystalline counterparts.

The AMR measurements are performed via the conventional 4-probe technique with the current flowing along the wire direction (also superimposed with the Fe[1 0 0] easy axis) (figure 5(*c*), inset). Four rectangular Au contact pads are deposited through a shadow mask across the wire arrays. The whole sample was mounted on an in-plane sample rotator to perform angular dependent $R(H)$ measurements. For parallel cooling and measurement, $R(H)$ stayed continuously at the high resistance level and showed no transitions during the whole magnetization reversal process, which indicates that the magnetization is either parallel or antiparallel to the direction of the current (figure 5(*c*)), consistent with the DW nucleation of magnetization reversal obtained in $M(H)$. For perpendicular cooling and measurement, at the descending branch, the magnetization gradually rotates along the wire axis (displaying high resistance) from the positive saturation field (displaying low resistance) as the field decreases, and finally rotates to the negative saturation field (displaying low resistance), which confirms that the magnetization reversal is via coherent rotation (figure 5(*d*)). We also measured the angular dependent $R(H)$ signals at 10 K for each cooling mode, with the magnetic field applied at an angle ϕ with respect to the current direction. ϕ is varied from 0° to 90° in steps of 10°. For both parallel cooling (H_{cool} along $\phi = 0°$) and perpendicular cooling (H_{cool} along $\phi = 90°$), $R(H)$ always stayed at high resistance level for $\phi \leqslant 50°$. Gradual changes of $R(H)$ signals can only be observed for $\phi > 50°$, figure 6. This indicates that the magnetization reversal mechanism changed from DW nucleation to coherent rotation at approximately $\phi = 50°$, which is consistent with the previous MOKE measurements [3].

5. Conclusion

We have demonstrated a thermal NIL process for the fabrication of large-area, submicron-size, epitaxial magnetic wires at high temperatures. The key to obtaining a high-quality liftoff during the fabrication process lies in generating the right undercut profile for the metallic Mo mask. This undercut is obtained, through carefully controlling dry etching and wet developing processes, from a distinctive wedge-shaped polymer resist profile. The utility of such patterning is illustrated using the magnetic properties of epitaxially grown *a*-axis Fe/MnPd wire arrays that were characterized by both VSM and AMR. Different magnetization reversal modes were found when magnetizing the sample along different orientations with respect to the wire axes. Small magnetization jumps are observed when measuring perpendicular to the wires, which are unique to our epitaxial samples. Notably, the reported technique is not limited to magnetism research but also promising for epitaxial NIL patterning purposes in other areas such as superconductors and multiferroics.

Acknowledgments

This work was supported by DoE/BES under contract no ER45987. Nanoimprint lithography and etching were performed at the Washington Technology Center Microfab Lab.

References

[1] Parkin S S, Hayashi M and Thomas L 2008 *Science* **320** 190

[2] Allwood D A, Xiong G, Faulkner C C, Atkinson D, Petit D and Cowburn R P 2005 *Science* **309** 1688

[3] Paz E, Cebollada F, Palomares F J, Garcia-Sanchez F and Gonzalez J M 2010 *Nanotechnology* **21** 255301

[4] Ciria M, Castano F J, Diez-Ferrer J L, Arnaudas J I, Ng B G, O'Handley R C and Ross C A 2009 *Phys. Rev.* B **80** 094417

[5] Hoffmann A, Grimsditch M, Pearson J E, Nogues J, Macedo W A A and Schuller I K 2003 *Phys. Rev.* B **67** 220406

[6] Chou S Y, Krauss P R and Renstrom P J 1996 *J. Vac. Sci. Technol.* B **14** 4129

[7] Hu W, Wilson R J, Xu L, Han S-J and Wang S X 2007 *J. Vac. Sci. Technol.* A **25** 1294

[8] Zhang W, Weiss D N and Krishnan K M 2010 *J. Appl. Phys.* **107** 09D724

[9] Suzuki N, Tanaka H, Yamanaka S, Kanai M, Lee B K, Lee H Y and Kawai T 2008 *Small* **4** 1661
[10] Givord D, Rossignol M and Barthem V M T S 2003 *J. Magn. Magn. Mater.* **258** 1
[11] Krishnan K M, Pakhomov A B, Bao Y, Blomqvist P, Chun Y, Gonzales M, Griffin K, Ji X and Roberts B K 2006 *J. Mater. Sci.* **41** 793
[12] Cheng N, Ahn J P and Krishnan K M 2001 *J. Appl. Phys.* **89** 6597
[13] Blomqvist P, Krishnan K M and McCready D E 2004 *J. Appl. Phys.* **95** 8019
[14] Blomqvist P, Krishnan K M, Srinath S and te Velthuis S G E 2004 *J. Appl. Phys.* **96** 6523
[15] Blomqvist P, Krishnan K M and Ohldag H 2005 *Phys. Rev. Lett.* **94** 107203
[16] Zhan Q F and Krishnan K M 2010 *J. Appl. Phys.* **107** 09D703
[17] Bruck S, Goering E, Schutz G, Ji X and Krishnan K M 2008 *Phys. Rev. Lett.* **101** 126402
[18] Zhan Q F and Krishnan K M 2010 *Appl. Phys. Lett.* **96** 112506
[19] Chung T Y and Hsu S Y 2008 *J. Appl. Phys.* **103** 07C506
[20] Ahn S H and Guo L J 2008 *Adv. Mater.* **20** 2044
[21] Weiss D N, Meyers S T and Keszler D A 2010 *J. Vac. Sci. Technol.* B **28** 823
[22] MicroChem Corp. LOR and PMGI resist http://www.microchem.com/products/pdf/PMGI-Resists-data-sheetV-rhcedit-102206.pdf
[23] Cowburn R P, Gray S J, Ferre J, Bland J A C and Miltat J 1995 *J. Appl. Phys.* **78** 7210
[24] Goolaup S, Singh N, Adeyeye A O, Ng V and Jalil M B A 2005 *Eur. Phys. J.* B **44** 259